ADVANCED FUNCTIONAL MATERIALS
www.afm-journal.de



# Low-Temperature Processable High-Performance Electrochemically Deposited p-Type Cuprous Oxides Achieved by Incorporating a Small Amount of Antimony

*Seung Ki Baek, Yong Hun Kwon, Jae Hui Shin, Ho Seong Lee, and Hyung Koun Cho**

**The development of an electrochemically robust method for the low-temperature deposition of cuprous oxide ($Cu_2O$) thin films with reliable and conductive p-type characteristics could yield breakthroughs in earth abundant and ecofriendly all oxide-based photoelectronic devices. The incorporation of the group-V element antimony (Sb) in the solution-based electrodeposition process has been investigated. A small amount of Sb (1.2 at%) in the $Cu_2O$ resulted in rapid nucleation and coalescence at the initial stage of electrochemical reaction, and finally made the surface morphology smooth in 2D. The growth behavior changed due to Sb addition and produced a strong diffraction intensity, single-domain-like diffraction patterns, and low angle tilt boundaries in the $Cu_2O$:Sb film, implying extremely improved crystallinity. As a result, these films exhibited extraordinary optical transmittance and band-to-band photoluminescence emission as well as higher electrical conductivity. The Cu/$Cu_2O$:Sb Schottky diode showed good rectifying characteristics and more sensible photoresponsibility.**

## 1. Introduction

Cuprous oxide ($Cu_2O$) is a natively p-type semiconductor known as an earth abundant and ecofriendly compound material with favorable optical properties for photoelectronic devices such as solar cells and photoelectrochemical cells. Suitable bandgaps and high absorption coefficient of the p-type $Cu_2O$ make it a good candidate as a photocathode for hydrogen evolution in water splitting systems.[1,2] Nevertheless, although the Shockley–Queisser limit for $Cu_2O$ is around 20% and the theoretical photocurrent is –14.7 mA $cm^{-2}$ under an AM 1.5 spectrum, the highest energy conversion efficiency of $Cu_2O$ is still below 5%.[1,3] One reason for the low efficiency is the high density of intrinsic defects in the $Cu_2O$ films, which create trap states and reduce minority carrier diffusion. These defects are generated from high grain boundaries and the nonuniform large grain size during the nucleation step, resulting in low hole mobility. Up to now, most $Cu_2O$ films for light-absorbing layers have had low electrical conductivity, which results in unfavorable band alignment and low short-circuit current.[4,5] Thus, $MoO_3$ and $V_2O_3$, which have appropriate band alignment, are mainly used as the hole transport layers (despite their n-type nature) instead of the p-type oxide.[6,7] The recent interest in stable p-type semiconductors without doping has focused on NiO, SnO, and $Cu_2O$.[8–10] However, among these, $Cu_2O$ alone is an excellent material that is able to provide a high hole mobility and high optical absorption efficiency in photoelectrical applications.[11]

Thus, to produce more conductive p-type $Cu_2O$, two approaches are available: i) doping acceptors in the $Cu_2O$ for high hole density, or ii) depositing the $Cu_2O$ with high crystalline quality for high hole mobility. It is well-known that p-type doping in metal oxides is typically challenging and doping characteristics are diminished by self- compensation.[12] Some transition metals and group V elements (e.g., nitrogen) have been shown to increase the p-type electrical conductivity. Lee et al., reported that nitrogen-doped $Cu_2O$ films grown by reactive sputtering have high carrier density and are a good hole transport layer.[13] However, to enhance the competitiveness of $Cu_2O$, the film deposition should also be compatible with low cost processes like solution-based sol–gel coating. Considering the excellent large-area uniformity, precursor recycling, low cost facilities, and low-temperature processing, electrochemical deposition using wet-based electrolytes is a very good choice.[14,15] In electrodeposition, the electrical conductivity can be tuned by controlling the pH and temperature,[16] but the variation is very limited, and the electrical conductivity of the $Cu_2O$ films is lower than the vacuum-processed $Cu_2O$. Unfortunately, doping in the electrodeposition process for the $Cu_2O$ films is more challenging due to limited dopants. The representative acceptor nitrogen is in the gas phase and cannot be effectively incorporated in solution processes because of the absence of adequate ionic solution precursors. Alternative dopants in metal

S. K. Baek, Y. H. Kwon, J. H. Shin, Prof. H. K. Cho
School of Advanced Materials Science and Engineering
Sungkyunkwan University
2066, Seobu-ro, Jangan-gu, Suwon,
Gyeonggi-do 440-746, Republic of Korea
E-mail: chohk@skku.edu
Prof. H. S. Lee
Department of Materials Science and Metallurgical Engineering
Kyungpook University
80 Daehakro, Buk-gu, Daegu 702-701, Republic of Korea

DOI: 10.1002/adfm.201501323

oxides, such as P and As, are also volatile and very toxic, and thus they also are naturally excluded in the solution process. In this work, a novel dopant, antimony (Sb) is used in the electrodeposition process for $Cu_2O$ films of high conductivity and high quality. In the electrodeposited $Cu_2O$ films, Sb is hypothesized to be one of the best choices for extrinsic doping because Sb is relatively ecofriendly, cost-effective, and nontoxic.[17] In addition, the application of Sb in the electrodeposition process has been actively utilized for the coating of $Sb_2Te_3$, $Sb_2Se_3$, and Sb layers.[18–20] There are currently no reports on the approach of Sb doping to achieve conductive $Cu_2O$ films in the wet processes.

In this work, we present a reliable p-type $Cu_2O$ thin film with more conductive p-type characteristics by incorporating a small amount of Sb in the electrochemical deposition process. The nucleation and growth evolution of the $Cu_2O$ layer has been experimentally investigated by employing electrochemical analyses. Consequently, the addition of a small amount of Sb in the $Cu_2O$ exhibited significantly improved crystalline quality and vertically well-aligned grain boundaries, resulting in enhanced electrical conductivity and optical properties. Also, we fabricated a Schottky junction photodetector to investigate the feasibility of low cost, ecofriendly, and wet-based processed oxide photoelectric devices.

## 2. Results and Discussion

During the depositions, we found that a small amount of Sb can be incorporated in the electrodeposited cuprous oxide without the precipitation of the Sb-related compounds. However, the addition of excess Sb precursor causes the formation of Sb precipitates to the bottom of the bottle, producing a murky ionic solution. **Figure 1** exhibits the typical current density–time transient curves during Sb-doped $Cu_2O$ ($Cu_2O$:Sb) and undoped $Cu_2O$ (u-$Cu_2O$) electrodeposition. These current transients can provide detailed information on the nucleation kinetics of

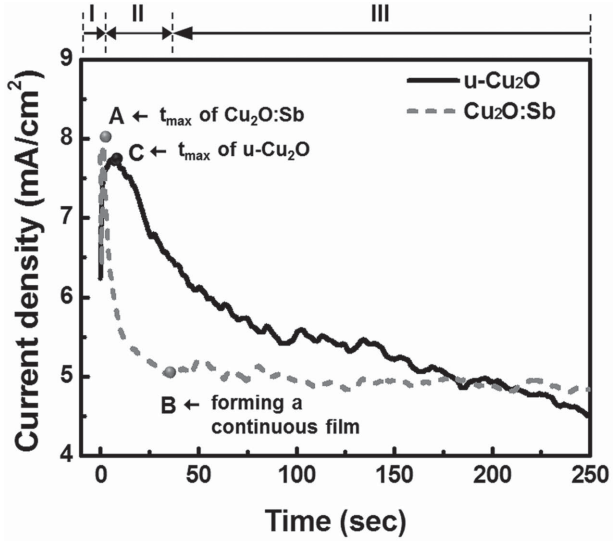


**Figure 1.** Typical current density–time transient curves for the $Cu_2O$:Sb and u-$Cu_2O$ electrodeposition to investigate the effect of Sb dopant addition on the electrochemical reaction.

cuprous oxide islands on the substrates and can aid in understanding the evolution of the surface morphology by analyzing the time dependence of the deposition current density.

Typically, in the current density–time transient, the current is high during the initial stage after double-layer charging, which indicates the growth of independent nuclei (region I). The current is maximized until the diffusion zones around all nuclei overlap. After that, the current decreased due to the impingement of growth centers, resulting in a decrease in the effective electrode surface area (region II), followed by a gradual approach to a steady state value by forming a 2D continuous layer (region III).[21] For the electrochemical analysis, the electrodeposition of cuprous oxide thin films was carried out in an aqueous solution of pH 11 and an applied potential of –0.4 V. Interestingly, the time corresponding to maximum current ($t_{max}$) for the $Cu_2O$:Sb is just below 1/4 of that for the u-$Cu_2O$, as shown in Figure 1, where $t_{max}$ in the $Cu_2O$:Sb electrodeposition is around 2 s (point A). This phenomenon is attributed to the acceleration of metal ion consumption close to the ITO substrate, which is known as the surfactant effect of the Sb metal ions.[22] Like highly strained III–V growth, the Sb as a surfactant in the electrodeposited $Cu_2O$ is expected to lower surface free energy and enhance the interaction between the substrate and adatoms, resulting in the increase of the nucleation density.[23] In addition, the total accumulated current density until $t_{max}$ (areal current density) becomes significantly reduced due to the low $t_{max}$ in the presence of Sb, which indicates that a small amount of Cu ions is consumed to achieve overlapping of all nuclei in the $Cu_2O$:Sb. These results suggest that the $Cu_2O$:Sb film has a higher nucleation density and smaller nuclei size than that of the u-$Cu_2O$. Moreover, it should be noticed that a steady saturation current density (region III, time >point B) is clearly observed in the presence of a small amount Sb, while the u-$Cu_2O$ exhibited a continuous decay of current density. This is because the initial $Cu_2O$ layer on the ITO substrate is grown with higher electrical resistivity, which agrees with previous studies.[24] Consequently, the incorporation of Sb in the electrodeposited cuprous oxides results in fast maximum current, reflecting the formation of fast nucleation and a diffusion zone. Finally, the deposition of 2D continuous films is expected.

As previously mentioned, the shorter $t_{max}$ is related to high nucleation density with small size nuclei, and contributes to the faster coalescence of these nuclei. **Figure 2** confirms our expectation regarding nucleation density and nuclei size, where the u-$Cu_2O$ and $Cu_2O$:Sb layers deposited at –0.4 V were compared after deposition times of 1, 6, and 20 s. The u-$Cu_2O$ deposition starts with the formation of sparse nuclei, ≈100 nm in diameter (Figure 2a). With increasing deposition time, these sparse nuclei grew to the larger $Cu_2O$ cubic crystals without the formation of a 2D film (Figure 2b,c). On the contrary, the $Cu_2O$:Sb deposition exhibits dense, small nuclei with a diameter range of 1–5 nm (Figure 2d). After a few seconds, the ITO substrate is fully and quickly covered with the $Cu_2O$:Sb, as shown in Figure 2e,f. It is well accepted that higher nucleation density and smaller nuclei size make the surface morphology smooth by fast coalescence. The time to complete film coverage is predominantly determined by the initial density of nuclei, and thus low nucleation density delays $t_{max}$ and causes larger island

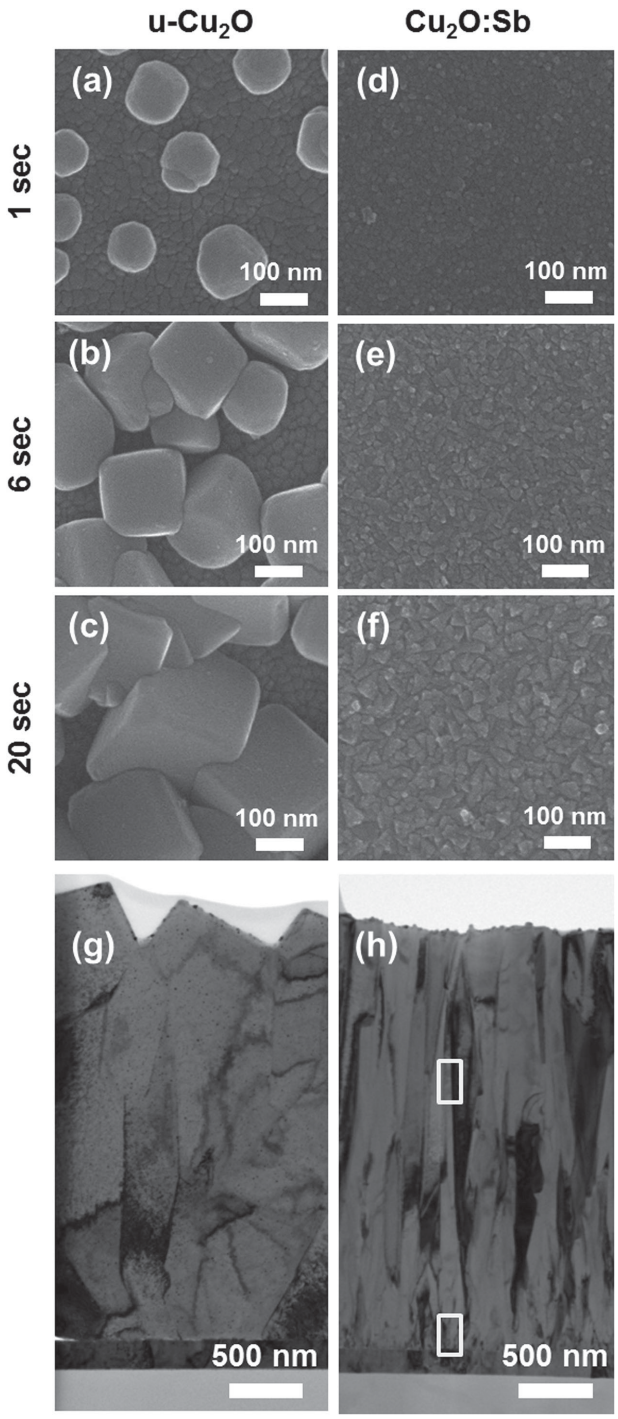


**Figure 2.** SEM images showing growth evolution at the initial stage for a–c) u-$Cu_2O$ and d–f) $Cu_2O$:Sb electrodeposition: a,d) 1 s, b,e) 6 s, c,f) 20 s. TEM bright-field images obtained from g) u-$Cu_2O$ and h) $Cu_2O$:Sb films.

size at $t_{max}$. In addition, the continuous decrease in the saturation current density in region III results from the formation of irregular facet-shaped crystals and the degraded electrical conductivity of these faceted $Cu_2O$ crystals. Most $Cu_2O$ films synthesized by electrodeposition have showed a large cubic shape with the {100} facets due to a slow growth rate with sufficient hydroxyl ions.[25] As a result, Figure 2g shows a sawtooth surface morphology with a segment width of ≈800 nm in the u-$Cu_2O$. However, the Sb-doped $Cu_2O$ with a low $t_{max}$, exhibited improved surface morphology with tiny segments on the nanometer scale. Therefore, we found that the addition of Sb in the cuprous oxide is a very effective approach in improving surface roughness without distinct facets.

According to previous reports, the fine grains near the substrate change to much coarser grains at greater distances from the substrate by rapid growth of low surface energy grains at the expense of high energy grains (Figure 2g).[26] Contrary to conventional microstructural evolution for columnar polycrystalline cuprous oxide, fine grains are also observed in the top region of the $Cu_2O$:Sb film, and grain boundaries are vertically well aligned from the substrate to the top region, as shown in Figure 2h. This indicates that the overlap of nuclei occurs fast for low thicknesses (low $t_{max}$), and the 2D-like layer-by-layer growth behavior is encouraged after the rapid formation of continuous films, resulting in the smooth surface morphology. The Sb elemental mapping via an aerial scan of EDS (Figure S1, Supporting Information) shows that Sb element is homogeneously distributed within the whole $Cu_2O$ film. It supports that the Sb addition retards lateral diffusion of Cu ions and growth along the other directions, and finally prevents the formation of larger grains via Oswald ripening. A schematic diagram explaining the effect of Sb incorporation on growth evolution is suggested in **Figure 3**. Consequently, slight Sb addition in the electrolyte with the same Cu ion concentration leads to an enormous change in nucleation and growth behavior of the cuprous oxides.

Prior to the potentiostatic electrodeposition, linear sweep voltammetry (LSV) was performed with a scan rate of 10 mV $s^{-1}$ to investigate the influence of Sb addition on the appropriate reaction potential range of the cuprous oxide thin films, as shown in **Figure 4**. The current–potential relationship is normally categorized as either a charge transfer or mass transport dominant reaction. In the charge transfer dominant process, the electrochemical reaction is controlled by the variation of overpotential, and the current density in the LSV curve is exponentially increased according to the Bulter–Volmer equation, showing how the electrical current at an electrode depends on the applied potential. On the contrary, under sufficient applied potential, mass transport determines the overall chemical reaction rate, and the current density in LSV is saturated to a constant value.[27] As shown in Figure 4, Sb incorporation leads to distinct charge transfer and mass transport limited reaction regimes as well as a mixed control mechanism. In particular, it is noticeable that in the case of $Cu_2O$:Sb, the mass transport growth mechanism is detected over a wide potential region (–0.35 to –0.65 V) with an almost constant current density, unlike the u-$Cu_2O$ film, which has a narrow constant current region (–0.64 to –0.69 V). In the Sb incorporated electrodeposition, a negative bias lower than –0.35 V immediately generates $Cu_2O$ products on the working electrode when electroactive species arrive in the diffusion boundary layer. The applied potential in this experiment was –0.4 V, and corresponds to the cathodic current densities of 3 mA $cm^{-2}$ (u-$Cu_2O$) and 5 mA $cm^{-2}$ ($Cu_2O$:Sb). Current density in the electrochemical reaction is proportional to the concentration of electroactive species according to following equation:

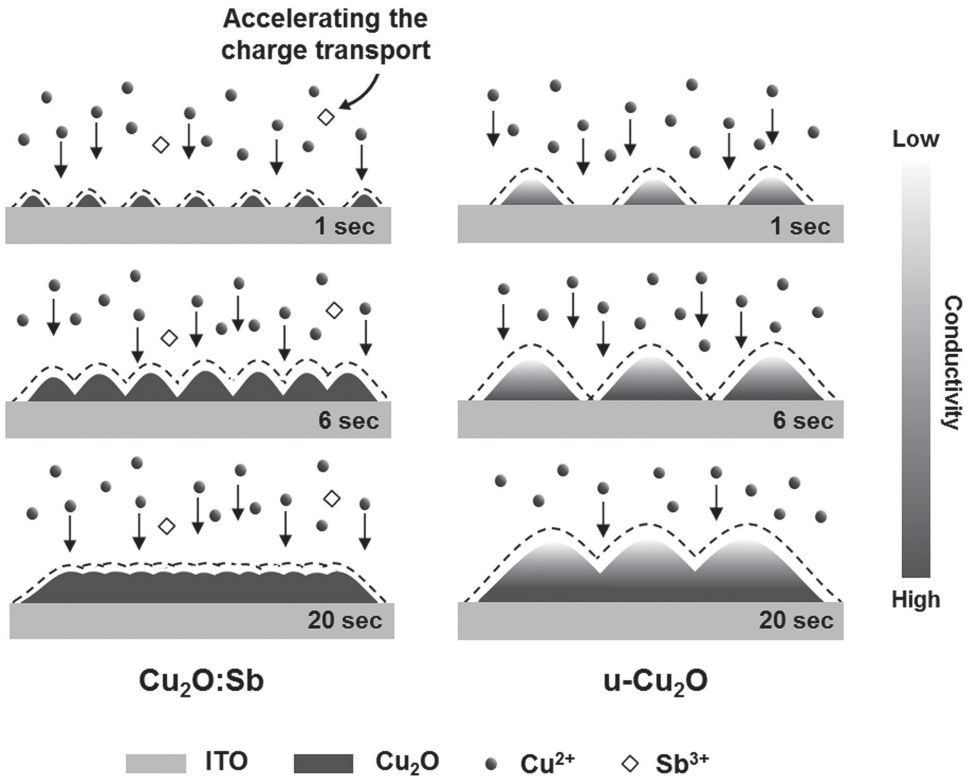


**Figure 3.** Schematic models showing the effect of Sb incorporation on growth evolution in the electrodeposited $Cu_2O$ thin films based on electrochemical analyses and SEM images.

$$I_L = \eta F k_D A c_b$$

where $I_L$, $\eta$, $F$, $k_D$, and $c_b$ indicate the limiting current, number of electrons involved, Faraday constant, diffusion coefficient, electrode area, and the concentration of metal ions in the bulk, respectively. Based on electrochemical data such as current–time transient and LSV, the addition of a small amount of Sb significantly affects the electrochemical reaction of the $Cu_2O$ films despite the low concentration (Sb/Cu = 0.005). These results reveal that the Sb addition accelerates charge transfer of $Cu^+$ ions to the diffusion layer. Additionally, the reaction under constant current with a long range plateau of –0.35 to –0.65 V follows the mass transport mechanism and promotes film growth along the vertical direction. Further, it suppresses abnormal reactions by the deviation of over potential during the electrochemical process and induces synthesis of stable and reproducible cuprous oxide.

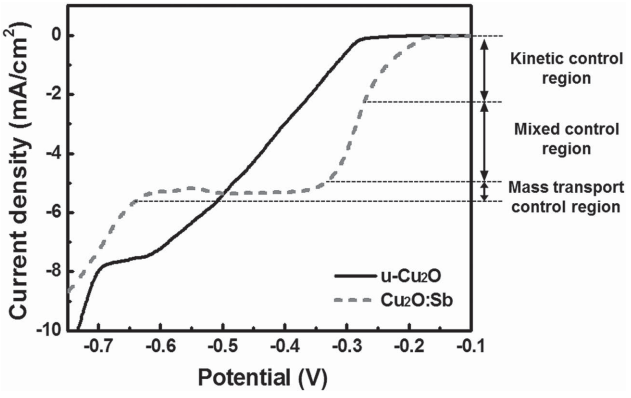


**Figure 4.** Linear sweep voltammetry (LSV) performed at a scan rate of 10 mV $s^{-1}$ for the $Cu_2O$:Sb and u-$Cu_2O$ electrodeposition.

We found that the addition of a small amount Sb in cuprous oxide considerably affects the electrochemical reaction, and thus we should investigate the effect of Sb doping on microstructural, optical, and electrical properties. First of all, we measured Sb content in the Sb-doped $Cu_2O$ synthesized using a concentration of $2 \times 10^{-3}$ M at 60 °C, and the amount of Sb was estimated to be approximately 1.2 at% from energy-dispersive X-ray spectroscopy (Figure S2, Supporting Information). **Figure 5**a illustrates X-ray diffraction (XRD) results of undoped and Sb-doped $Cu_2O$ films deposited on the ITO/glass substrates, and all diffraction peaks can be indexed as a pure $Cu_2O$ phase. There are no diffraction peaks from Sb metal and Sb-related alloys. Typically, in a solution pH of >11, the $Cu_2O$ (111) surface shows much faster growth by consuming more oxygen atoms per unit area than the (100) and (110) surfaces.[28] Thus, polycrystalline $Cu_2O$ films are generally deposited with the (111) preferred orientation at pH 11, and the exposed facets consist of {100} faces with a relatively slow growth rate. The most salient difference due to the Sb addition in the XRD results is the extremely strong diffraction intensity and decreased full width at half maximum (FWHM) of the (111) orientation. The integrated intensity is enhanced by at least 32 times. This variation in XRD intensity of a single diffraction peak generally occurs when the film is changed from a preferred polycrystal

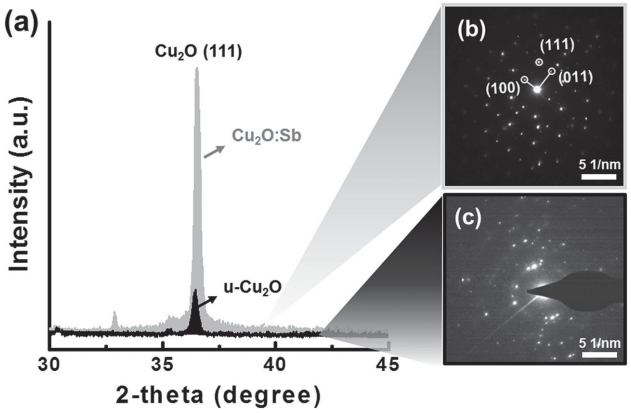


**Figure 5.** a) XRD patterns of $Cu_2O$:Sb and u-$Cu_2O$ films. b) Selected area diffraction patterns obtained from b) u-$Cu_2O$ and c) $Cu_2O$:Sb films.

orientation to a single-crystal-like domain. As such, this indicates a considerable improvement in the crystallinity of $Cu_2O$ film. Transmission electron microscope (TEM) analyses were performed to confirm the improved crystallinity. Selected area electron diffraction (SAED) patterns of the u-$Cu_2O$ and $Cu_2O$:Sb thin films are shown in Figure 5b,c, respectively. A notable feature observed in the $Cu_2O$:Sb is the absence of arc-shaped diffraction patterns from the typical polycrystalline with preferred orientation. Rather, distinct spot diffraction patterns were observed like the SAED from single-domain crystals. Here, the SAED from the $Cu_2O$:Sb was indexed with a zone axis of [$\bar{1}$10]. As explained previously, the u-Cu2O films on the ITO substrates are composed of large facets with a sawtooth shape. However, the addition of a small amount Sb exhibits narrow grains with vertically well- aligned grain boundaries from the substrate, as observed in TEM images (Figure 2h). The TEM image for the $Cu_2O$:Sb film seems to suggest a polycrystalline structure, while the SAED looks like a single domain or a large grain. Thus, we performed high-resolution TEM on the $Cu_2O$:Sb film to evaluate atomic arrangement of the boundary between adjacent grains.

**Figure 6**a–d shows high-resolution TEM (HR-TEM) images obtained from the bottom and middle regions of the $Cu_2O$:Sb, respectively, as marked by rectangles in Figure 2h. The initial grains of the $Cu_2O$:Sb on the ITO substrate have a random crystal orientation, where the $Cu_2O$ (200) planes with an interplanar spacing of 0.21 nm were oriented along the different directions. However, after sufficient deposition, the HR-TEM image shows the (111) oriented domains well aligned with the interplanar spacing of 0.25 nm. It is expected that the Sb accelerates the growth along the [111] direction of the $Cu_2O$ and suppresses the growth along the other directions. In addition, the crystal grains in the middle region show low angle tilt boundaries of approximately ≈3° of the (100) planes, as shown in Figure 6c,d. These TEM results reveal that the Sb addition induced a strong (111) preferred orientation along the vertical direction and slightly tilted crystal domains along the in-plane direction. As a result, the XRD showed an extremely intense (111) peak with a narrow FWHM and the SAED resembled single-crystal-like spot patterns, despite being polycrystalline.

After the synthesis of the $Cu_2O$:Sb, we were greatly amazed at the sample color. The general cuprous oxide film has a direct bandgap of 2.1 eV, a high absorption coefficient, and high density of grain boundaries. These properties resulted in an opaque film. Our reference $Cu_2O$ film also showed a transmittance of ≈10% in the 700–800 nm wavelength, as shown in **Figure 7**a. However, we can obviously distinguish letters under the $Cu_2O$:Sb film with 3 μm thickness by the naked eye, and this film exhibits a high optical transmittance exceeding 70% above 650 nm wavelength. The bandgap of 2.1 eV induces a reddish semitransparent film. Among various p-type oxide semiconductors, photoluminescence (PL) is barely observed with the exception of doped ZnO. In addition, because of the self-compensation effects of the ZnO, it is difficult to obtain good emission properties in stable p-type oxides. In the $Cu_2O$ films based on a high vacuum process, a few reports about PL results have been published, but there are no reports on PL emission from solution-processed $Cu_2O$ films. As shown in Figure 7b, the PL emission from the $Cu_2O$:Sb film at room temperature was so obvious that a bright red color could be clearly seen by the naked eye in air, while the u-$Cu_2O$ film showed no emission. To check the stability of the PL characteristics, the PL was investigated under

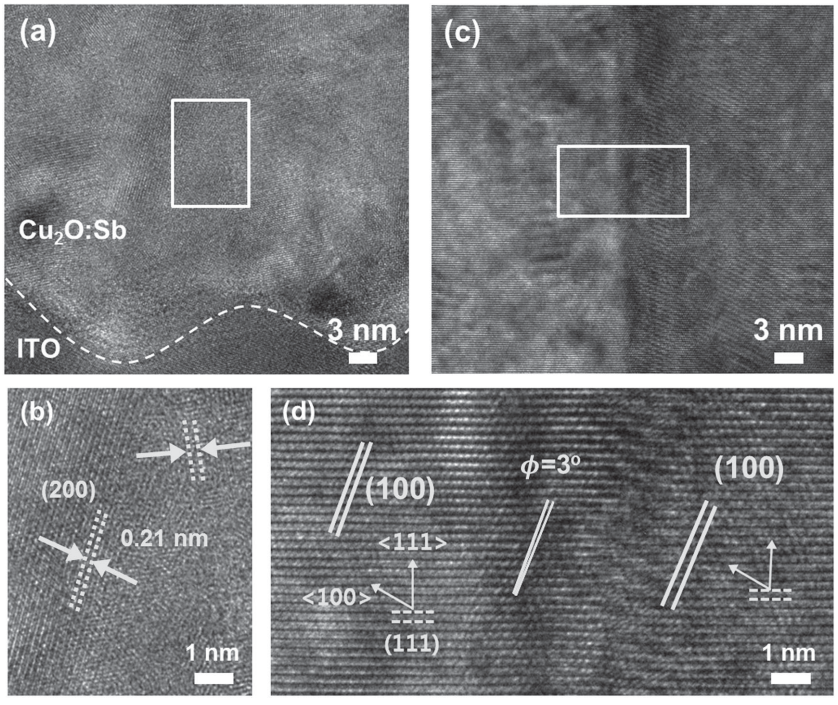


**Figure 6.** HR-TEM images obtained from the a,b) bottom and c,d) middle regions of the $Cu_2O$:Sb, as marked by rectangles in Figure 2h. Here, (b) and (d) are magnified images of (a) and (c).

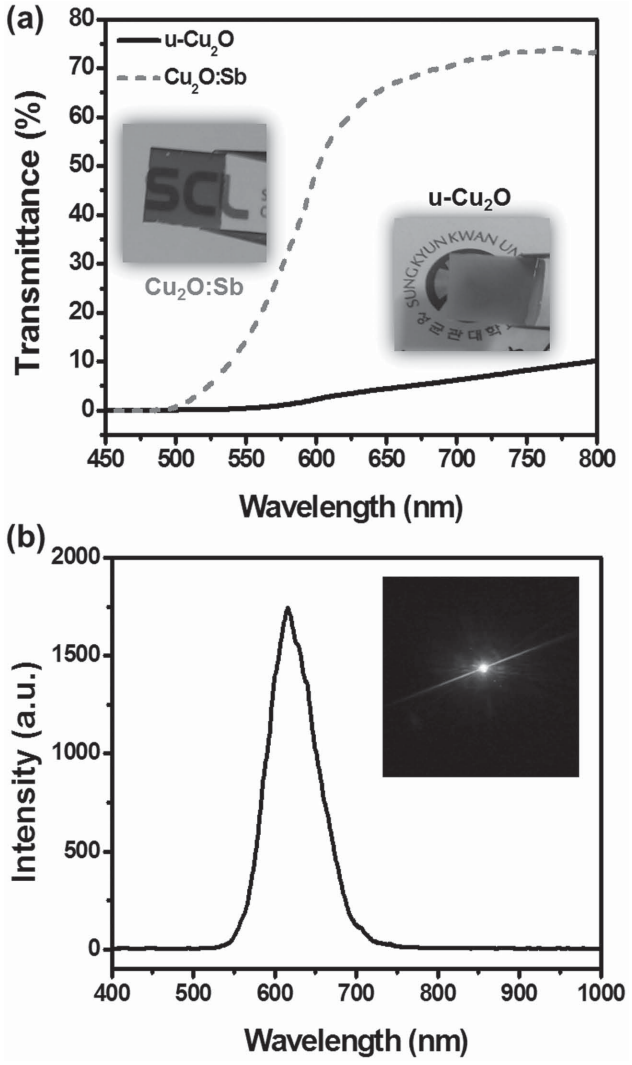


**Figure 7.** a) Optical transmission spectra of $Cu_2O$:Sb and u-$Cu_2O$ films. The inset images show obvious underlying letters under the $Cu_2O$:Sb film with 3 μm thickness observed by the naked eye. b) PL spectrum recorded from the $Cu_2O$:Sb film at room temperature. The inset shows distinguishable emission color.

the same environment after 15 d, and the distinct emission was strongly observed without optical and electrical degradation. The PL peak was positioned at 620 nm and corresponded to a band-to-band transition of the $Cu_2O$, considering the bandgap of the $Cu_2O$. Other $Cu_2O$ films deposited under vacuum exhibited deep level emission known to be due to charged oxygen and copper vacancies.[29] These special optical characteristics are believed to originate from the formation of high crystalline quality $Cu_2O$:Sb films with a strong (111) preferred orientation and low tilt angle grain boundaries, which results in a decrease in light scattering and nonradiative recombination.

To investigate the electrical properties of the $Cu_2O$:Sb film, Hall-effect measurements were performed at room temperature. Prior to the measurement, u-$Cu_2O$ and $Cu_2O$:Sb films are detached using epoxy resin pellets for the elimination of the conductive ITO substrate. These electrodeposited $Cu_2O$ films show obvious p-type characteristics, which were confirmed by

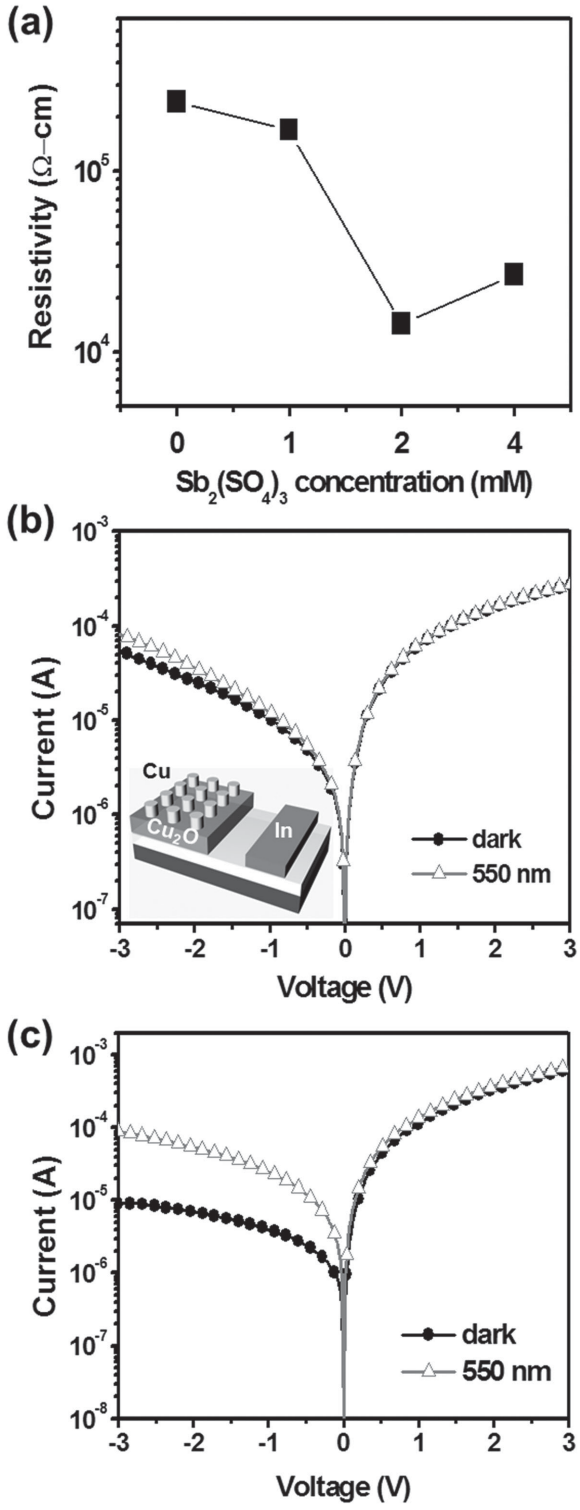


**Figure 8.** a) Electrical resistivity as a function of the Sb mole concentration in the solution obtained from Hall-effect measurement. *I–V* characteristics from b) Cu/u-$Cu_2O$ and c) Cu/$Cu_2O$:Sb Schottky diodes under dark and green illumination (550 nm).

photoelectrochemical and Hall measurements (Figure S3 and Table S1, Supporting Information). **Figure 8** shows the variation of electrical resistivity depending on the Sb mole concentration

of the solution. The electrical resistivity of $Cu_2O$ film decreased from $2.4 \times 10^5$ to $1.4 \times 10^4$ Ω cm by adding $2 \times 10^{-3}$ M Sb sulfate in a cupric bath, which corresponds to the reduction of one order. After the addition of Sb, the carrier concentration was maintained around $10^{13}$ $cm^{-3}$, and the Hall mobility was significantly increased from 2.1 to 28.5 $cm^2$ $V^{-1}$ $s^{-1}$. It is known from Lee et al., that this observation is the result in low potential barriers at low angle grain boundaries.[30] Low angle grain boundaries reduced the potential barrier that blocked charge carrier transport between adjacent grains compared to randomly rotated grain boundaries. The enhancement in the electrical conductivity is attributed to the increase in hole charge mobility, not carrier density. Therefore, the role of a small amount of Sb addition is not electrical doping, but the formation of $Cu_2O$ films with reduced defect density through stable mass transport reaction in the electrochemical deposition. Thus, this result reveals that the substitution of Sb for oxygen sites is not effective. Furthermore, the $Cu_2O$:Sb film shows high electrical stability without variation in electrical properties after 6 months.

In order to utilize p-type Sb-doped $Cu_2O$ oxide semiconductors with improved electrical properties and high stability in photonic devices, we fabricated a $Cu_2O$-based Schottky junction photodiode. In particular, it is difficult for the $Cu_2O$ films electrodeposited on the ITO to be used in various fabrication processes such as ultrasonic agitation, wet treatments, and post-thermal annealing, due to poor adhesion between the film and substrate. However, the Sb-added $Cu_2O$ films do not show these mechanical and thermal treatment related problems any more. Thus, we attempted to fabricate various device structures. Among several electrode metals, 200 nm Cu (work function of ≈4.5 eV) was used as a Schottky contact with the p-type $Cu_2O$, where the Schottky photodiode requires a metal electrode with a lower work function.[31] The photoresponse of the 550 nm green light was evaluated and the current–voltage characteristics for the photodetector of the u-$Cu_2O$ and $Cu_2O$:Sb films are shown in Figure 8b,c, respectively. The I(illumination)/I(dark) ratio at −3 V of the u-$Cu_2O$ film is around 1.6, indicating the low photoresponsivity. In contrast, the $Cu_2O$:Sb film exhibits a current ratio of >10. The Cu/$Cu_2O$:Sb Schottky diode shows an enhanced forward current and lower leakage current, indicating good rectifying characteristics. In the Schottky photodiodes, 550 nm light illumination generates photocarriers in the depletion region of the p-type $Cu_2O$ region. On the contrary, the movement of the photocarriers in the u-$Cu_2O$ layer is suppressed by its short minority carrier diffusion length caused by the highly tilted grain boundaries and the interface defects at the Schottky junction expected in the sawtooth surface.[4,32] Although the doping concept of p-type $Cu_2O$ using Sb ions does not effectively provide substitutional hole carriers, the electrochemical deposition offers an interesting approach to grow highly crystalline and extremely stable p-type $Cu_2O$ by incorporating Sb dopant. In addition, these results open up new possibilities for the fabrication of all oxide-based photoelectronic devices by developing an electrically stable p-type oxide at quite a low temperature (<100 °C).

## 3. Conclusion

We have developed a novel electrochemical route for the realization of low temperature processable high performance p-type $Cu_2O$ films. The incorporation of a small amount of Sb produced a significant improvement in the structural and optical properties of the electrodeposited $Cu_2O$ films through high nucleation density with small sizes and a fast coalescence process. We have comparatively discussed growth evolution and smooth surface morphology using electrochemical and microstructural analyses. The $Cu_2O$:Sb films consisted of the vertically well-aligned grains with low angle tilted boundaries, and exhibited an intense and single-domain-like diffraction peak. Our $Cu_2O$:Sb films showed a reduction of one order in electrical resistivity, which was not attributed to the substitution of Sb for oxygen sites but rather to enhanced mobility (28.5 $cm^2$ $V^{-1}$ $s^{-1}$) from the extreme improvement in crystal quality. Additionally, semitransparent characteristics ($T \approx 70\%$) and optical emission at 620 nm were obtained from the Sb-doped $Cu_2O$. To fabricate fundamental photoelectronic devices using p-type $Cu_2O$:Sb with improved electrical properties and high stability, we made a Cu/$Cu_2O$ Schottky photodetector and the I(illumination)/I(dark) ratio from Cu/$Cu_2O$:Sb showed a ≈10 times higher value due to the high crystalline quality and enhanced carrier mobility.

## 4. Experimental Section

*Growth of u-$Cu_2O$ and $Cu_2O$:Sb Films by Electrodeposition*: Commercially available ITO (sheet resistance of 10 Ω $sq^{-1}$ and thickness of 180 nm) coated on a glass substrate was used as working electrode in a three-electrode system for electrodeposition at 60 °C. The $Cu_2O$ films were grown on ITO by electrochemical deposition in an aqueous Cu electrolyte consisting of 0.4 M copper (II) sulfate anhydrous (Junsei, >98%) and 3 M lactic acid (Sigma-Aldrich, 85%) as a stabilizer agent. The pH of the solution was adjusted to 11 by adding a 4 M sodium hydroxide solution. For the $Cu_2O$:Sb films, antimony sulfate (Sigma-Aldrich, >98%) was added in the chemical bath with different concentrations of (0–4) $\times 10^{-3}$ M. Here, a platinum mesh with a high surface area and an Ag/AgCl (saturated NaCl) were used as a counter electrode and a reference electrode (+ 0.194 V vs normal hydrogen electrode, NHE), respectively. The amount of Sb is ≈1.2 at% in ionic concentrations of $2 \times 10^{-3}$ M. $Cu_2O$ and $Cu_2O$:Sb films were potentiostatically electrodeposited at −0.4 V to obtain an electric charge of 3 C $cm^{-2}$ with a Princeton Applied Research Versatate 4.

*Performance Analysis of u-$Cu_2O$ and $Cu_2O$:Sb Films*: The morphology of the $Cu_2O$ thin films was examined using a field-emission scanning electron microscope (FE-SEM, JSM-6700F, 10 kV) and a (TEM, Titan G2, 200 kV). XRD analyses were performed to characterize the crystallinity of the films using a Bruker AXS D8 Discover with a Cu K$\alpha$ radiation source (1.5405 Å). Optical transmittance spectra were measured using a UV–vis–NIR spectrophotometer (Varian Cary 5000), and PL spectra were confirmed using a He–Cd laser operating at a wavelength of 325 nm. Electrical properties including electrical resistivity and carrier mobility were evaluated with a Hall effect measurement system with a magnetic field of 0.55 T applied perpendicular to the sample surface. For the Hall effect measurement, the electrodeposited films were transferred to an epoxy resin (Torr seal, Varian) by a mechanical method.[33] To characterize the photoelectric properties, Cu metal electrodes were deposited on the surface of the $Cu_2O$ films by sputtering. I–V measurements were carried out in the dark and under 550 nm illumination using an HP-4145B and a 150 W Xenon arc lamp (Oriel) as a light source.

## Supporting Information

Supporting Information is available from the Wiley Online Library or from the author.

## Acknowledgements

This research was supported by the Basic Science Research Program through the National Research Foundation of Korea (NRF) funded by the Ministry of Science, ICT and Future Planning (Grant No. 2015R1A2A2A01007409).

Received: April 2, 2015
Revised: June 11, 2015
Published online: July 14, 2015

[1] A. Paracchino, V. Laporte, K. Sivula, M. Grätzel, E. Thimsen, *Nature* **2011**, *10*, 456.
[2] Z. Zhang, R. Dua, L. Zhang, H. Zhu, H. Zhang, P. Wang, *ACS Nano* **2013**, *7*, 1709.
[3] Y. S. Lee, M. T. Winkler, S. C. Siah, R. Brandt, T. Buonassisi, *Appl. Phys. Lett.* **2011**, *98*, 192115.
[4] K. P. Musselman, A. Marin, L. Schmidt-Mende, J. L. MacManus-Driscoll, *Adv. Funct. Mater.* **2012**, *22*, 2202.
[5] S. K. Baek, K. Y. Lee, H. K. Cho, *J. Nanomater.* **2013**, 421371
[6] D. W. Zhao, P. Liu, X. W. Sun, S. T. Tan, L. Ke, A. K. K. Kyaw, *Appl. Phys. Lett.* **2009**, *95*, 153304.
[7] M. Yu, X. Liu, Y. Wang, Y. Zheng, J. Zhang, M. Li, W. Lan, Q. Su, *Appl. Surf. Sci.* **2012**, *258*, 9554.
[8] J. H. Lee, Y. H. Kwon, B. H. Kong, J. Y. Lee, H. K. Cho, *Cryst. Growth Des.* **2012**, *12*, 2495.
[9] Y. Ogo, H. Hiramatsu, K. Nomura, H. Yanagi, T. Kamiya, M. Hirano, H. Hosono, *Appl. Phys. Lett.* **2008**, *93*, 032113.
[10] S. Y. Kim, C. H. Ahn, J. H. Lee, Y. H. Kwon, S. Y. Hwang, J. Y. Lee, H. K. Cho, *ACS Appl. Mater. Interfaces* **2013**, *5*, 2417.
[11] B. S. Li, K. Akimoto, A. Shen, *J. Cryst. Growth* **2009**, *311*, 1102.
[12] Y. Y. Kim, W. S. Han, H. K. Cho , *Appl. Surf. Sci.* **2010**, *256*, 4438.
[13] Y. S. Lee, J. Heo, M. T. Winkler, S. C. Siah, S. B. Kim, R. G. Gordon, T. Buonassisi, *J. Mater. Chem. A* **2013**, *1*, 15416.
[14] A. Paracchino, J. C. Brauer, J. E. Moser, E. Thimsen, M. Grätzel, *J. Phys. Chem. C* **2012**, *116*, 7341.
[15] K. Mizuno, M. Izaki, K. Murase, T. Shinagawa, M. Chigane, M. Inaba, A. Tasaka, Y. Awakura, *J. Electrochem. Soc.* **2005**, *152*, C179.
[16] K. Han, M. Tao, *Sol. Energy Mater. Sol. Cells* **2009**, *93*, 153.
[17] Y. N. Sandana, J. P. Singh, R. Kumar, *Surf. Technol.* **1985**, *24*, 319.
[18] G. Leimkuhler, I. Kerkamm, R. Reineke-Koch, *J. Electrochem. Soc.* **2002**, *149*, C474.
[19] T. T. Ngo, S. Chavhan, I. Kosta, O. Miguel, H. J. Grande, R. Tena-Zera, *ACS Appl. Mater. Interfaces* **2014**, *6*, 2836.
[20] Y. Zhang, G. Li, Y. Wu, B. Zhang, W. Song, L. Zhang, *Adv. Mater.* **2002**, *14*, 1227.
[21] H. Majidi, K. T. Van, J. B. Baxter, *J. Electrochem. Soc.* **2012**, *159*, D605.
[22] H. Cao, D. Lu, J. Lin, Q. Ye, J. Wu, G. Zheng, *Electrochim. Acta* **2013**, *91*, 234.
[23] X. Yang, J. B. Heroux, M. J. Jurkovic, W. I. Wang, *Appl. Phys. Lett.* **2000**, *76*, 7
[24] C. M. Mcshane, W. P. Siripala, K. S. Choi, *J. Phys. Chem. Lett.* **2010**, *1*, 2666.
[25] L. C. Wang, N. R. Tacconi, C. R. Chenthamarakshan, K. Rajeshwar, M. Tao, *Thin Solid Films* **2007**, *515*, 3090.
[26] M. Paunovic, M. Schlesinger, *Fundamental of Electrochemical Deposition*, 2nd ed., John Wiley & Sons, Inc., Hoboken, NJ, USA **2006**, Ch. 7.
[27] C. Ponce-de-Leon, C. T. J. Low, G. Kear, F. C. Walsh, *J. Appl. Electrochem.* **2007**, *37*, 1261.
[28] W. Zhao, W. Fu, H. Yang, C. Tian, M. Li, Y. Li, L. Zhang, Y. Sui, X. Zhou, H. Chen, G. Zou, *CrystEngComm* **2011**, *13*, 2871.
[29] H. Solache-Carranco, G. Juarez-Diaz, A. Esparza-Garcia, M. Briseno-Garcia, M. Galvan-Arellano, J. Martinez-Juarez, G. Romero-Paredes, R. Pena-Sierra, *J. Lumin.* **2009**, *129*, 1483.
[30] S. Y. Lee, W. J. Lee, C. W. Nahm, J. M. Kim, S. J. Byun, T. H. Hwang, B. K. Lee, Y. I. Jang, S. E. Lee, H. M. Lee, B. W. Park, *Curr. Appl. Phys.* **2013**, *13*, 775
[31] F. Shao, J. Sun, L. Gao, J. Luo, Y. Liu, S. Yang, *Adv. Funct. Mater.* **2012**, *22*, 3907.
[32] A. K. Ghosh, C. Fishman, T. Feng, *J. Appl. Phys.* **1980**, *51*, 446
[33] T. Shinagawa, M. Chigane, K. Murase, M. Izaki, *J. Phys. Chem. C* **2012**, *116*, 15925.